# Ferroelectricity Induced by Acentric Spin-Density Waves in YMn2O5

Chapon, L.C.; Radaelli, P.G.; Blake, G.R.; Park, S.; Cheong, S.-W.

*Published in:*
Physical Review Letters

*DOI:*
10.1103/PhysRevLett.96.097601



*Publication date:*
2006

# Ferroelectricity Induced by Acentric Spin-Density Waves in $YMn_2O_5$

L. C. Chapon,[1] P. G. Radaelli,[1,2] G. R. Blake,[1,3] S. Park,[4] and S.-W. Cheong[4]

[1]*ISIS Facility, Rutherford Appleton Laboratory-CCLRC, Chilton, Didcot, Oxfordshire, OX11 0QX, United Kingdom*
[2]*Department of Physics and Astronomy, University College London, Gower Street, London WC1E 6BT, United Kingdom*
[3]*Materials Science Division, Argonne National Laboratory, Argonne, Illinois 60439, USA*
[4]*Department of Physics and Astronomy, Rutgers University, Piscataway, New Jersey 08854, USA*

(Received 7 November 2005; published 7 March 2006)

The commensurate and incommensurate magnetic structures of the magnetoelectric system $YMn_2O_5$, as determined from neutron diffraction, were found to be spin-density waves lacking a global center of symmetry. We propose a model, based on a simple magnetoelastic coupling to the lattice, which enables us to predict the polarization based entirely on the observed magnetic structure. Our data accurately reproduce the temperature dependence of the spontaneous polarization, particularly its sign reversal at the commensurate-incommensurate transition.

DOI: 10.1103/PhysRevLett.96.097601 PACS numbers: 77.80.−e, 61.12.−q, 75.25.+z, 75.30.Fv

There is currently great interest in understanding the microscopic nature of the coupling between ferroelectricity and magnetic ordering in several transition metal oxides, such as $R\mathrm{MnO_3}$ and $R\mathrm{Mn_2O_5}$ ($R$ = rare earth element) [1–6]. This coupling is responsible for the sensitivity of these materials to an applied magnetic field and may lead to new classes of functional materials. Unlike more conventional multiferroics such as $\mathrm{BiFeO_3}$ and $\mathrm{BiMnO_3}$, the paramagnetic phase in these new materials is centrosymmetric, and electrical polarization appears only at the transition to a magnetically ordered phase. This implies that the ordered spin structure is responsible for removing the center of symmetry and generating a polar field. Two approaches have so far been proposed in the literature: The magnetoelastic effect could occur through a *scalar* field of the type $S_n \cdot S_{n+1}$, which must be coupled to a preexisting polar field from the crystal structure, or through a *vector* field of the type $S_n \times S_{n+1}$ [6–8]. In the latter case, noncollinearity is a key ingredient to promote a polar state, whereas in the former case a collinear phase could, in principle, support electrical polarization. Naturally, in both cases, global inversion symmetry must be lost.

Recently, we showed that, for $\mathrm{TbMn_2O_5}$ [3], the largest electric polarization is associated with a commensurate magnetic (CM) state that is almost collinear. The magnetic structure can be described as a superposition of several amplitude-modulated waves on inequivalent lattice sites with noncoincident nodal points, making it acentric (the structure has constant moments for an appropriate choice of the global phase). On further cooling below 25 K, the $\mathrm{TbMn_2O_5}$ magnetic structure becomes incommensurate (ICM) with $\mathbf{k} \sim (0.48, 0, 0.32)$. Although the electrical polarization evolves in a complex way through this transition, the ICM phase remains ferroelectric, displaying, at low temperatures, a remarkably strong coupling with an applied magnetic field [2]. It is therefore of great interest to solve the ICM structure and determine how global inversion symmetry is lost, since in a simple spin-density wave (SDW) one can always find a lattice point that is also an inversion center. On the basis of theoretical considerations and experimental data, Kenzelmann and co-workers [5] propose that in $\mathrm{TbMnO_3}$ inversion symmetry is broken by the development of a cycloidal magnetic structure, which can be described as a superposition in quadrature of two waves associated with different components of the magnetic moment on the *same* site. Here we propose a different and, to our knowledge, hitherto unexplored mechanism for the ICM phases of the $R\mathrm{Mn_2O_5}$ series: The loss of inversion symmetry arises from the superposition of two waves on *different* crystallographic sites, each with an independent phase factor. In the specific case of $\mathrm{YMn_2O_5}$, where we have solved both CM and ICM structures from neutron diffraction data, we show that the temperature dependence of the electrical polarization as calculated from the magnetic structure using a simple $S_n \cdot S_{n+1}$ exchange coupling is consistent with the measurement of electrical properties [9]. In particular, our model is capable of reproducing the sign reversal of the polarization observed at the CM-ICM transition [9].

$\mathrm{YMn_2O_5}$ is isostructural to $\mathrm{TbMn_2O_5}$ and shows the same sequence of magnetic transitions and electrical anomalies upon cooling, but the analysis of the magnetic structures is considerably simplified by the absence of magnetism on the rare earth site. Magnetic ordering appears below 45 K with a CM vector and switches to an ICM state below 23 K. Similar to $\mathrm{TbMn_2O_5}$, the ferroelectric state coexists with the magnetically ordered state, and, at the first-order CM-ICM transition, the dielectric constant jumps to higher values whereas the spontaneous electrical polarization is reversed and decreases in amplitude to about 25% of its original value [9]. Polycrystalline $\mathrm{YMn_2O_5}$ was prepared by conventional solid-state reaction in an oxygen environment. Neutron powder diffraction data were collected using the general materials diffractometer at the ISIS facility. Data were recorded on warming from 1.9 to 53 K in 2 K steps using a helium cryostat. A collection time of 2 hours was used at 1.9 K in order to

 

obtain high statistics data in the saturated ICM regime and 20 minutes for all other temperatures. Data analysis was performed with the program FULLPROF [10]. Magnetic structures were determined by using global optimization techniques (simulated annealing) for data collected at, respectively, 1.9 and 24.7 K followed by final Rietveld refinements at all temperatures. During simulated annealing runs, the magnetic moments on equivalent Mn sites were constrained to be equal.

The crystal structure of $YMn_2O_5$ refined at 53 K, space group *Pbam*, is in perfect agreement with previous studies on isostructural $RMn_2O_5$, ($R$ = Tb, Ho, Dy) [4]. As for other members of the series, there is no evidence of crystal symmetry breaking from neutron diffraction at low temperature, due to the extremely weak atomic displacements involved. Below 45 K, the data show the appearance of magnetic Bragg peaks, which can be indexed with a CM propagation vector $\mathbf{k} = (1/2, 0, 1/4)$ above 23 K and with an ICM $\mathbf{k} \sim (0.48, 0, 0.29)$ below 17 K. The transition between CM and ICM states, marked by the coexistence of both magnetic phases, is of first-order type. A small discontinuous reduction of the magnetic signal is also observed on warming through the ICM-CM transition. The combined structural-magnetic Rietveld refinements, shown in Fig. 1 for data at 24.7 and 1.9 K, are of very good quality, with magnetic reliability factors of 5.6% and 5.5% and $\chi^2$ of 4.4 and 16.3 (the higher value is due to the longer collection time). The corresponding magnetic structures are displayed in Fig. 2, and complete lists of parameters are reported in Table I. In the CM phase, the spin

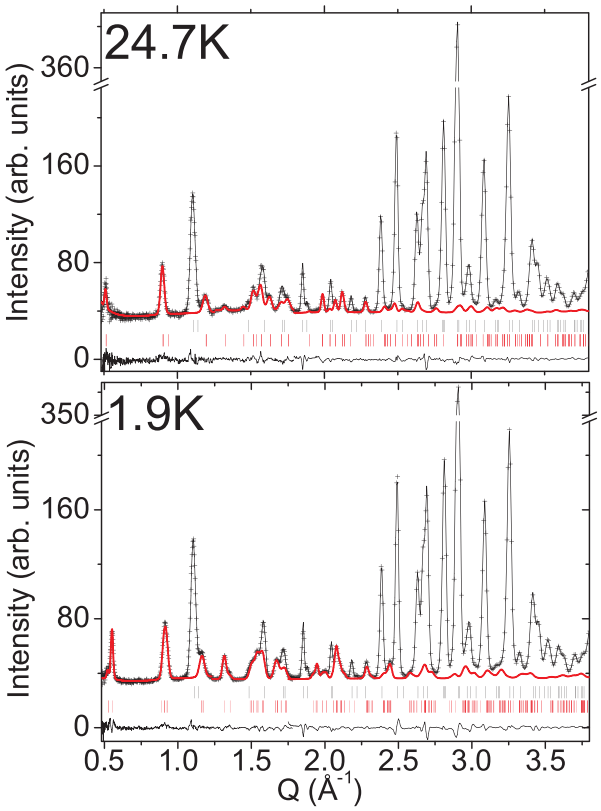


FIG. 1 (color online). Rietveld refinements at 24.7 and 1.9 K. Data sets from 3 detector banks located at 18, 35, and 63.6° $2\theta$ are merged on the same scale. The cross points and solid lines show the experimental data points and calculated profile, respectively. The difference is shown on the bottom as solid lines. The upper and lower rows of markers indicate, respectively, the positions of the nuclear and magnetic reflections. The light gray/red solid line emphasizes the calculated magnetic contribution.

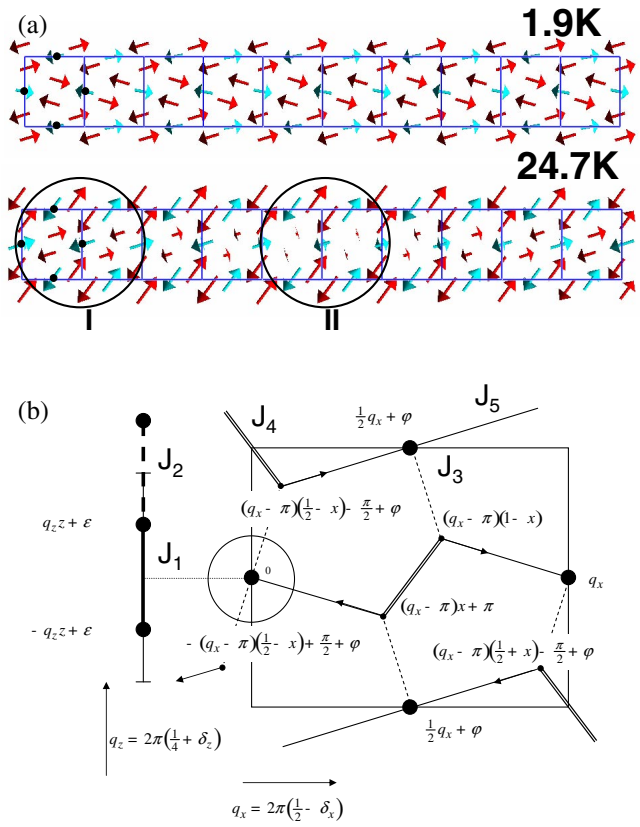


FIG. 2 (color online). (a) Magnetic structure at 24.7 (top) and 1.9 K (bottom) projected in the *ab* plane. Ten unit cells are displayed along *a*. For clarity, a single $Mn^{4+}/Mn^{3+}$ layer is shown. The arrows represent the magnetic moment on $Mn^{4+}$ (blue), at positions marked by black dots, and $Mn^{3+}$ (red). For the ICM structure, region I is locally very similar to the CM phase (both chains having sizable moments) and does not contain inversion centers. Region II could potentially contain an inversion center and is described in more detail in (b) and in the text. (b) A schematic representation of the magnetic structures of both CM and ICM phases (see text). The fragment on the left side represents a portion of the ... $Mn^{4+}$-$Mn^{4+}$ ... chains along the *c* axis. The SDW phases are as shown in the labels of the $Mn^{3+}$ sites and are obtained for the $Mn^{4+}$ sites by adding the values of the *a*- and *c*-axis projections. The arrows indicate the direction of the underlying *centrosymmetric* vector field that is coupled to the magnetism and coincides with the axes of the $Mn^{3+}O_5$ pyramids. Magnetic exchange pathways are also indicated.

arrangement, corresponding to an amplitude modulation, is similar to that found for $TbMn_2O_5$ [3]. The spins, directed in the $ab$ plane, are antiferromagnetically aligned along $\ldots Mn^{4+} \ldots Mn^{3+}Mn^{3+} \ldots Mn^{4+} \ldots$ chains running along the $a$ axis. We note that, within a chain, each $Mn^{3+}$ ion is connected to two $Mn^{4+}$ located in layers at $z \sim 0.25$ and $(1 - z)$, an important detail (see below) that is difficult to represent in the projected structure. There are two antiferromagnetic ''chains'' per unit cell [3]. The moments on the $Mn^{3+}$ and $Mn^{4+}$ sites are oriented at respective angles of 10(5)° and 15(5)° to the $a$ axis. The spins on $Mn^{4+}$ sites at $z \sim 0.25$ and $(1 - z)$, connected through the $Mn^{3+}$ layer, are ferromagnetically aligned. A magnetic structure with constant moments, as shown in Fig. 2(a), can be obtained when the phases are set to $\pm\pi/4$ (see below and also Table I).

The ICM magnetic structure at 1.9 K also corresponds to a sinusoidal modulation of the moments (Fig. 2). However, this phase is a true SDW, since every amplitude value is realized on each crystallographic site. An unconstrained refinement of the initial model found by simulated annealing shows that magnetic moments on sites related by the glide plane operation are phased by values close to $\frac{1}{2}k_x$ ($k_x = 0.479$ being the component of the propagation vector along $a^*$). This leads to an almost exact cancellation of the magnetic moment in one of the chains when the moments in the other chain are fully ordered. The refinement also indicates that $Mn^{4+}$ atoms at $z \sim 0.25$ and $(1 - z)$ positions, unrelated by symmetry operations of the group of the propagation vector, have phase shifts of almost $\frac{1}{2}k_z$, with $k_z = 0.291$. The moments in one of the chains are at an angle of 15(4)° to the $a$ axis, similar to that observed in the CM phase, while the direction of the moments in the other chain is tilted by 56(4)°. This model implies the superposition of the two irreducible representations (irreps) of the paramagnetic group, as allowed in the case of a first-order transition. The observed canting is consistent with magnetic susceptibility data [9]: The CM phase has $b$ and $c$ as almost equal ''easy'' magnetic directions. At the CM-ICM transition, $b$ becomes a harder axis, while $a$ becomes an easier axis, again in agreement with our magnetic structure showing a rotation of half of the chains towards the $b$ axis. There are no anomalies in the susceptibility along $c$ at the CM-ICM transition.

A unified description of both CM and ICM structures, consistent with the experimental data within the errors, is shown in Fig. 2(b). Phases on each crystallographic site within a chain have been assigned so that the moments follow a single harmonic modulation (their amplitude being related to their $x$ fractional coordinate). The phases of the waves on adjacent chains are allowed to vary from being exactly opposite, the global phase shift between them being denoted as $\varphi$. Along $c$, the moments also follow a sinusoidal modulation (their amplitude being related to the fractional coordinate $z' = z - \frac{1}{2}$), with a phase shift $\epsilon$ with respect to the origin. We have deliberately chosen the origin of the plot to coincide with an inversion symmetry point of the ICM modulation along the $a$ axis for $\varphi = 0$ and $\epsilon = 0$. The CM constant-moment phase is obtained by setting the incommensurability parameters $\delta_x$ and $\delta_z$ and the phase shift $\epsilon$ to zero and by setting $\varphi = \pi/2$ [Fig. 2(b)]. It is clear by construction that the ICM phase is noncentrosymmetric for $\epsilon \neq 0$ and $\varphi \neq 0$. The relationship between the CM and ICM phases is also illustrated in Fig. 2(a). The CM phase corresponds to a local region of the ICM phase that does not contain centers of symmetry.

The value of the *net* electrical polarization along the $b$ axis (i.e., averaging over the oscillating components) is easily calculated based on the contribution of the symmetric interchain exchange interaction to the magnetoelastic coupling described in Ref. [3] and the phase factors of Fig. 2(b):

$$P^{\mathrm{ICM}} = 4C\vec{S}_3 \cdot \vec{S}_4 \cos(2\pi(\tfrac{1}{4} + \delta_z)z') \cos(2\pi\delta_x(\tfrac{1}{2} - x)) \times \cos(\epsilon)\sin(\varphi), \quad (1)$$

where $\vec{S}_3$ and $\vec{S}_4$ are the magnetic moments on the $Mn^{3+}$ and $Mn^{4+}$, respectively, and $C$ is the magnetoelastic coupling constant. The polarization has been obtained by

TABLE I. Magnetic parameters obtained from Rietveld refinements of the 1.9 and 24.7 K data.

| | | 24.7 K | | | 1.9 K | | |
|---|---|---|---|---|---|---|---|
| Atom | Position | $M_x(\mu_B)$ | $M_y(\mu_B)$ | Phase (rad) | $M_x(\mu_B)$ | $M_y(\mu_B)$ | Phase (rad) |
| $Mn^{4+}$ | (0 0.5 0.255) | 3.092(9) | −0.5(2) | $\frac{\pi}{4}$ | −3.46(8) | −0.9(1) | −0.459 |
| $Mn^{4+}$ | (0.5 0 0.255) | −3.092(9) | −0.5(2) | $\frac{\pi}{4}$ | −1.9(2) | −3.0(1) | 4.15(69) |
| $Mn^{4+}$ | (0 0.5 0.745) | 3.092(9) | −0.5(2) | $\frac{\pi}{4}$ | −3.46(8) | −0.9(1) | 0.459 |
| $Mn^{4+}$ | (0.5 0 0.745) | −3.092(9) | −0.5(2) | $\frac{\pi}{4}$ | −1.9(2) | −3.0(1) | 5.09(69) |
| $Mn^{3+}$ | (0.412 0.351 0.5) | −3.63(9) | −1.0(2) | $\frac{\pi}{4}$ | −4.02(8) | −1.0(2) | 2.83(44) |
| $Mn^{3+}$ | (0.588 0.649 0.5) | 3.63(9) | 1.0(2) | $\frac{\pi}{4}$ | −4.02(8) | −1.0(2) | −0.31(44) |
| $Mn^{3+}$ | (0.088 0.851 0.5) | 3.63(9) | 1.0(2) | $\frac{\pi}{4}$ | −2.5(2) | −3.3(2) | 1.44(81) |
| $Mn^{3+}$ | (0.912 0.149 0.5) | 3.63(9) | 1.0(2) | $\frac{\pi}{4}$ | −2.5(2) | −3.3(2) | 1.44(81) |

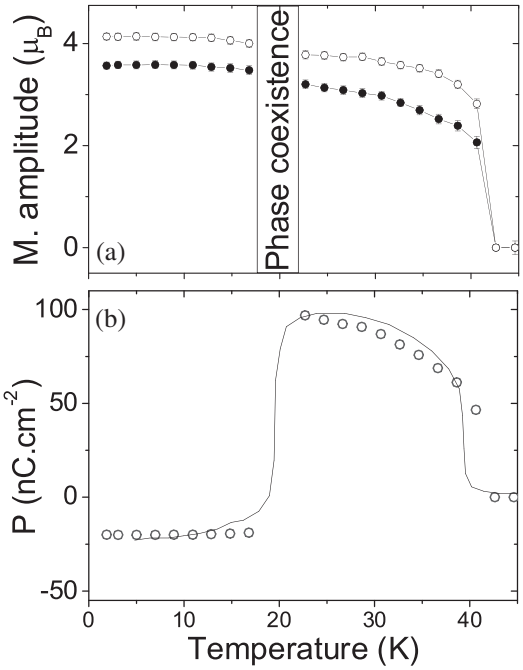


FIG. 3. (a) Refined values of the magnetic wave amplitudes on $Mn^{3+}$ (open symbols) and $Mn^{4+}$ (solid symbols) as a function of temperature. The *average* moment on each site is $\frac{1}{\sqrt{2}}$ of the wave amplitude. (b) Symbols: Electrical polarization of $YMn_2O_5$, as calculated from Eq. (1). Solid line: Experimental values of the electrical polarization, extracted from Kagomiya *et al.* [9]. The calculated polarization has been scaled by a single constant to account for the unknown magnetoelastic coupling parameter.

multiplying the magnetic terms by the *b*-axis component of the underlying polar field, shown with arrows in Fig. 2(b). From Eq. (1), it is clear that a nonzero value of the phase $\varphi$ is required to promote a *b*-axis polarization. This is only possible if both irreps are involved, since for each irrep $\varphi = 0$ by symmetry. In addition, the polarization direction can change depending on the value of $\varphi$.

With the help of Eq. (1) and the experimental values of the phases (Table I), we can predict the value of the polarization for the ICM phase. In practice, however, the error bars on the magnetic phases for an individual measurement introduce a large uncertainty on the value of the calculated polarization. To overcome this, we have fitted the weak temperature dependence of the ICM phases, to obtain constant phase differences. These yield a polarization of *opposite sign* and reduced by approximately a factor of 5 with respect to the CM phase, in close agreement with the experimental values determined by Kagomiya *et al.* [9]. The temperature dependence of the spontaneous polarization has been calculated and is shown in Fig. 3 to be in good agreement with the experimental curve by Kagomiya and co-workers [9].

Although $\varphi \neq 0$ is clearly allowed by symmetry in our case, and as we have shown this can lead to a spontaneous polarization of either sign in the ICM phase, it is presently unclear to us how a nonzero value can be energetically favorable. In fact, in the simple isotropic exchange model, the interchain energy can be written as:

$$E_3^{\mathrm{ICM}} = -4J_3\vec{S}_3 \cdot \vec{S}_4 \cos(2\pi(\tfrac{1}{4} + \delta_z)z') \sin(2\pi\delta_x(\tfrac{1}{2} - x)) \times \cos(\epsilon)\cos(\varphi), \quad (2)$$

which is even in $\varphi$. It is noteworthy, however, that $E_3^{\mathrm{ICM}}$ is linear in $\delta_x$ for small $\delta_x$, suggesting a natural mechanism to stabilize the incommensurability along the *a* axis.

In summary, we have developed a model to explain the presence of ferroelectricity in the CM and ICM phases of $YMn_2O_5$ *without* the need to invoke noncollinearity and/or chirality as essential features. We show that ferroelectricity is compatible with an acentric SDW, which the literature reports as the most probable magnetic structure for this class of materials [11,12]. We have determined the high-temperature commensurate and low-temperature incommensurate magnetic structures of $YMn_2O_5$ based on neutron diffraction data. The calculated electrical polarization based on our model and a simple magnetoelastic coupling was found to be in good agreement with the experimental values at all temperatures, including a previously unexplained sign reversal at the CM-ICM transition.

We acknowledge helpful discussions with Daniel Khomskii, Maxim Mostovoy, and Joseph Betouras. Work at Rutgers was supported by NSF-DMR-0520471.

[1] T. Kimura, T. Goto, H. Shintani, K. Ishizaka, T. Arima, and Y. Tokura, Nature (London) **426**, 55 (2003).
[2] N. Hur, S. Park, P. A. Sharma, J. Ahn, S. Guha, and S.-W. Cheong, Nature (London) **429**, 392 (2004).
[3] L. C. Chapon, G. R. Blake, M. J. Gutmann, S. Park, N. Hur, P. G. Radaelli, and S.-W. Cheong, Phys. Rev. Lett. **93**, 177402 (2004).
[4] G. R. Blake, L. C. Chapon, P. G. Radaelli, S. Park, N. Hur, S.-W. Cheong, and J. Rodriguez-Carvajal, Phys. Rev. B **71**, 214402 (2005).
[5] M. Kenzelmann, A. B. Harris, S. Jonas, C. Broholm, J. Schefer, S. B. Kim, C. L. Zhang, S.-W. Cheong, O. P. Vajk, and J. W. Lynn, Phys. Rev. Lett. **95**, 087206 (2005).
[6] W. Ratcliff, II, V. Kiryukhin, M. Kenzelmann, S.-H. Lee, R. Erwin, J. Schefer, N. Hur, S. Park, and S.-W. Cheong, Phys. Rev. B **72**, 060407(R) (2005).
[7] I. A. Sergienko and E. Dagotto, cond-mat/0508075.
[8] G. Lawes *et al.*, Phys. Rev. Lett. **95**, 087205 (2005).
[9] I. Kagomiya, S. Matsumoto, K. Kohn, Y. Fukuda, T. Shoubu, H. Kimura, Y. Noda, and N. Ikeda, Ferroelectrics **286**, 167 (2003).
[10] J. Rodriguez-Carvajal, Physica (Amsterdam) **192B**, 55 (1993).
[11] C. Wilkinson, F. Sinclair, P. Gardner, J. B. Forsyth, and B. M. R. Wanklyn, J. Phys. C **14**, 1671 (1981).
[12] P. P. Gardner, C. Wilkinson, J. B. Forsyth, and B. M. Wanklyn, J. Phys. C **21**, 5653 (1988).